Inverse Design Methodology for Patient Specific Soft Robotics

Mark D Gilbertson,[1] James D Van de Ven,[2] and Timothy M Kowalewski[3]

***Abstract*— We propose a methodology of inverse design for soft robotic actuators. This approach could be used to create designs of patient-specific catheter robots that may achieve behaviors not possible with existing catheter approaches. Specifically, given an initial robot shape (e.g. a tube like a typical catheter) and a nearly arbitrary desired final shape (e.g. a bend or spiral shape as dictated by patient-specific anatomy), what is the material design to realize this actuation? To accomplish a material design tools from differential geometry and continuum mechanics are applied to soft robotics. A material dithering algorithm is proposed to enable 3D printing of designs with a finite set of elastomeric materials. Bending and spiral shapes are used as a case study, resulting in credible designs based on a qualitative review of the design results.**

I. Introduction

Soft robotics has empowered robots to maneuver, traverse, and complete tasks where traditional rigid robots cannot. The soft nature of these robots allows them to conform to unknown dynamic environments and operate within a multitude of tight spaces, within debris sites, tubes, and the human body [1]. Traditionally soft robots rely on forward design. That is, given a manufacturing process and motion mechanism like inflation under the antagonistic priciple [2], [3] or concentric tubes [4], [5], the designer must innovate to within the resulting design space to hopefully achieve an actuator or robot that meets a specific task. This could limit application areas and yield suboptimal performance of the soft robot as the specific choice of the process and mechanism constrain the design space. Inverse design on the other hand is grounded first in the specific task or tasks and directly yields theoretical robot geometry required to meet the task requirements. The manufacturing process can be a secondary consideration; inverse design would inform or inspire a suitable manufacturing process rather than assume one must be selected a priori.

Inversely designed soft robots could be used to create patient-specific robots. Two potential applications are 1) vessel traversal for tortuous vessels that existing catheters cannot negotiate or 2) filling a cavity for reconstruction such as a major vessel under aneurysm repair. By creating patient specific actuators cardiovascular "no option" patients—individuals whose vasculature is incompatible with any existing catheters and who are ineligible for bypass surgery—could potentially be cleared for an intravascular intervetion. This would require a method that given two shapes, would yield a robot geometry that moves from the initial shape to the final shape. The initial shape could be a simple cylindrical tube typical of catheters and the final shape could be a patient-specific geometry. Currently, there exists no technique for the inverse design of a soft robot that can actuate from such a specified initial shape to a final shape. For example, the "pulling catheter" motion descried in [6] and shown anchored in a vessel with two spiral actuators in Fig. 1 would be advantageous over traditional cathetes in navigating tortuous vessels as it would require less anatomical forces to advance the catheter. However, the fiber-reinforced implementation in [6] limits the ultimate design space and cannot decouple design variables like overal longitudinal strech and radial stretch. Ideally, the desired shapes are simply dictated by the task and a suitable robot design should result.

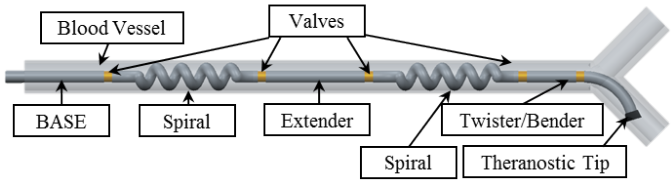

Fig. 1: Soft robot locomoting through a cannula. The robot consists of a tethered base and five segments, each containing a valve and an actuator. The spiral shapes prevent blockage of blood flow while anchoring to the lumen wall. The extender expands in length when the hydraulic pressure is applied into the actuator producing locomotion. The twister and bender allows the robot to navigate through junctions and provide theranostics to the cannula. The cap represents the end effector.

The overall goal of this work is to make a general method for the inverse design of soft fluid powered actuators from pre-specified shapes. Specifically, given an initial robot shape (e.g. a tube) and desired final shape (e.g. as dictated by patient-specific anatomy), what is the material design to realize this actuation? To accomplish a material design tools from differential geometry and continuum mechanics are applied to soft robotics. While continuum mechanics has been utilized in soft robotics [7] [8] it has not been used for inverse design.

The specified shapes will be constructed by parameterizing analytic functions. First, each shape's centerline will define a spine function. Then Frenet-Serret parameterization will be used to wrap a surface around the spine to create an arbitrary tubular shape. The Cauchy-Green Strain tensor will

[1]Department of Mechanical Engineering, University of Minnesota, 111 Church St. Minneapolis, MN gilbe767@umn.edu

[2] Associate Professor of Mechanical Engineering, University of Minnesota, 111 Church St. Minneapolis, MN

[3] Assistant Professor of Mechanical Engineering, University of Minnesota, 111 Church St. Minneapolis, MN

then be applied to show local deformation at any point of the actuator as the well as the Cauchy stress tensor and a neo-Hookean constitutive law. With these tools, given two actuator shapes required by a specific task, a soft robot with distal locomotion can be inversely designed. And, given an appropriate manufacturing process like multimaterial elastomeric additive manufacturing, the design can potentially be realized.

II. Methods

1) Mathematical Tools for Inverse Design: The first step of achieving inverse design was to create a mathematical framework to represent the desired initial and final shapes. Notation was created which defines an initial and final shape as well as dictate the stretch between the shapes. To create the shapes, a spine function (the centerline of a tubular shape) was defined and Frenet-Serret formulas was used from differential geometry to create a 3D surface. This approach is illustrated as two case studies: a) a bending actuator (e.g. for a specific turn radius in a vessel) and b) a spiral actuator (e.g. for anchoring and pulling through a patient-specific geometry, see [6]). Both shapes originate as simple cylindrical tubes.

First a spine function was created. The spine is a straight line for the initial shape and a deformed shape like a circular arc in the final configuration. A circular and helical spine, Ω, are given in eq. 1 and eq. 2 respectively.

$$\Omega_{circle}(t) = \begin{bmatrix} \frac{L}{\alpha} sin(\alpha t) \\ 0 \\ \frac{L}{\alpha} cos(\alpha t) - \frac{L}{\alpha} \end{bmatrix} \tag{1}$$

$$\Omega_{helix}(t) = \begin{bmatrix} Rcos(kt/2\pi) \\ Rsin(kt/2\pi) \\ tL_z \end{bmatrix} \tag{2}$$

Where t is parameterization along the length. L is arc length of the spine. α is the angle of bending of the spine. R is the helix radius. L_z is length of the spiral in the z-direction. k is pitch of the spiral.

With spines created, the next step was to create a tubular structure to encase the spine. Frenet-Serret parameters were chosen as they find the normal (**N**) and binormal (**B**) direction of the tangent spine (**T**) and allow a circle to be created perpendicular to the spine at any point. Eq. 3 describes the resulting deformation, φ.

$$\varphi(\mathbf{X}) = \Omega(t) + r(cos(\theta)\mathbf{N}(t) + sin(\theta)\mathbf{B}(t)) \tag{3}$$

Where θ is the parameterization around the spine and $\mathbf{X}$ represents X, Y, Z before the transformation.

2) Actuator Stretch Mapping: In order to determine the stretch mapping from the initial actuator pose to a specified actuator pose Continuum Mechanics was utilized. The deformation gradient and left and right Cauchy-Green tensors (eq. 4) and the first three strain invariants (eq. 5) of the deformation (eq. 3) was be taken at any point along the actuator.

$$\mathbf{F} = \frac{\partial \varphi(\mathbf{X})}{\partial \mathbf{X}} \quad \mathbf{C} = \mathbf{F}^T\mathbf{F} \quad \mathbf{B} = \mathbf{F}\mathbf{F}^T \tag{4}$$

$$I_1 = tr(\mathbf{B}) \quad I_2 = \tfrac{1}{2}[(tr(\mathbf{B}))^2 - tr(\mathbf{B}^2)] \quad I_3 = det(\mathbf{B}) \tag{5}$$

3) Task 1: Stiffness Mapped Geometry: The next step was to calculate the required material stiffness given a hydrostatic pressure, p. In order to use a constraint on the hydrostatic pressure we assumed a thin wall and treated the stress analysis as if it were a shell.

The Cauchy stress tensor (eq. 6) can be used to define the stress as a function of the deformation and constitutive law. An isotropic neo-Hookean material (eq. 7) was assumed which allowed for the reduction of eq. 6 with eq. 8.

$$\sigma = \frac{1}{I_3}[I_3 W_{,I_3}\mathbf{I} + 2(W_{,I_1} + I_1 W_{,I_2})B - 2W_{,I_2}B^2] \tag{6}$$

$$W = c_1(I_1 - 3) \tag{7}$$

$$W_{,I_1} = c_1 \quad W_{,I_2} = 0 \quad W_{,I_3} = 0 \tag{8}$$

The hydrostatic pressure can be represented by decomposing the Cauchy stress tensor into devatoric (shear) and hydrostatic pressure components. This representation is shown in eq. 9 where s is the devatoric portion. Eq. 9 can be rewritten in terms of only the σ and p by taking a trace which removes the devatoric components (eq. 10).

$$\sigma = s - pI \tag{9}$$

$$p = -\frac{1}{3}tr(\sigma) \tag{10}$$

Substituting eq. 6-8 into eq. 10 produces an equation for the neo-Hookean material constant as a function of the deformation and input pressure (eq. 11).

$$c_1 = \frac{3p}{2tr(B)} \tag{11}$$

While this method was shown for a neo-Hookean material it could be expanded to higher ordered material models while still adhering to the method presented and outlined in Algorithm 1.

4) Task 2: Material Mapping: With a stiffness mapped geometry determined (eq. 11) the next goal was to determine a finite number of materials to represent the stiffness. Volumetric dithering algorithms, similar to a Floyd-Steinberg algorithm [9], was applied to the stiffness mapped geometry to produce a dithered mapping. This dithered mapping took a stiffness mapped geometry, determined the 10th and 90th percentile of stiffness and dithered between these two values as shown in Algorithm 2 producing a dithered geometry.

Algorithm 1 Volumetric Stiffness Mapping Algorithm

procedure STIFFNESS_MAP(F, p)
    Cauchy stress, σ
    Select constitutive law, W
    Simplify σ with W
    Apply $p = -\frac{1}{3}tr(\sigma)$
    solve for material coefficients
end procedure

Algorithm 2 Modified Floyd-Steinberg Material Dithering

procedure DITHER(c_1)
    for y from top to bottom **do**
        for x from left to right **do**
            mat_choice := find_closest_mat(c_1[x][y])
            ξ[x][y] := mat_choice
            E := c_1[x][y] - mat_choice
            ξ[x+1][y] := c_1[x+1][y] + E * 7/16
            ξ[x-1][y+1] := c_1[x-1][y+1] + E * 3/16
            ξ[x][y+1] := c_1[x][y+1] + E * 5/16
            ξ[x+1][y+1] := c_1[x+1][y+1] + E * 1/16
        end for
    end for
    return(ξ)
end procedure

*Constants derived for globally minimized error [9].
mat() stands for material

III. Results

To test both cases the actuator design in Table I was used.

TABLE I: Actuator parameters used to fulfill eq. 1-3.

r	L	α	R	L_z	k
10 mm	100 mm	90 deg	7.5 mm	100 mm	1

For both spine selections eq. 1 and eq. 2 a continuous and dithered stiffness mapped geometry was found. Figure 2 and Figure 3 both show the mappings and conditions respectively. Table II show the 10th and 90th percentile of the continuous stiffness mapping for the bending and spiral actuator.

TABLE II: Material coefficients used in Algorithm 1

Percentile	Bender	Spiral
10^{th}	37.748 kPa	2.2385 kPa
90^{th}	37.860 kPa	2.2386 kPa

IV. Discussion

Figure 2 shows the tubular actuator before and after the specified deformation. Figure 2a-b show the actuator with a continuous stiffness mapping. This mapping follows one's intuition of a bending actuator and is similar to the corresponding design in [10]. After the dithering had been performed (Figure 2c-d) it can be seen that the continuous and dithered geometry follow intuitive trends.

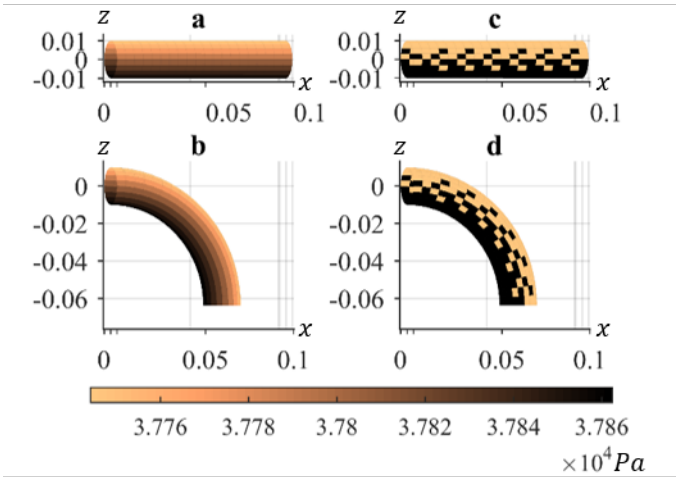

Fig. 2: Continuous and dithered stiffness mappings of a bending actuator (case a). The first order continuous stiffness mapping are shown in **a** and **b** while the binary dithered material mapping from Algorithm 2 and Table II is shown in **c** and **d**. All distances are in meters.

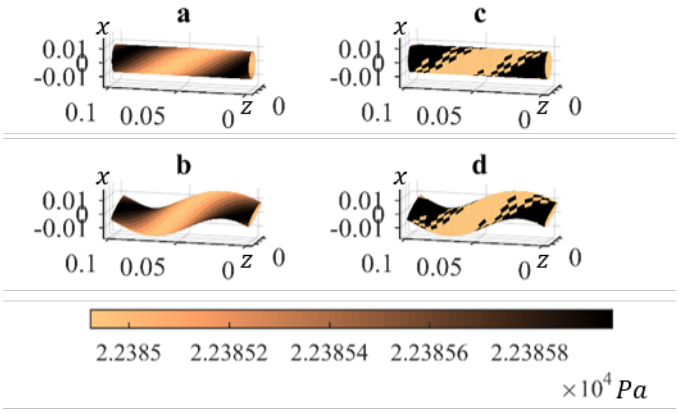

Fig. 3: Continuous and dithered stiffness mappings of a spiraling actuator (case b). The first order continuous stiffness mapping are shown in **a** and **b** while the binary dithered material mapping from Algorithm 2 and Table II is shown in **c** and **d**. All distances are in meters.

Figure 3 shows the design from a spiraling actuator of the same radius of the bending actuator. By looking at the both the dithered and continuous mapping one can intuitively see how the actuators could deform from Figure 3a to Figure 3b or Figure 3c to Figure 3d.

The model presented makes the assumption that the wall thickness is infinitesimally thin. This neglects an important factor in computing resulting stresses from strains. This is likely partly the cause of the the derived material parameters to have a small range as seen in Table II and for their values to be low. While this creates issues for realistic FEM simulation, it still provides a proof-of-concept for the

material mapping. To address this, wall thickness must be explicitly included in the shape models and deformation mapping.

The shapes selected with eq. 1-3 have issues with compressibility. In order for this method to be fully valid it should enforce incompressibility with $det(F) = 1$. To guarantee incompressibility a volume preservation method will be used. First the initial and final volume of each deformed and undeformed element will be set equal to each other. Then an equation relating the final thickness will be solved for as a function of the initial thickness, as well as the initial and final length and radius.

V. Conclusion

We presented an inverse design methodology to shape specific material mappings for tubular actuators. While this method is still in its infancy and requires additional modeling, most notably with the inclusion of thickness and guarantee of incompressibility, the method was able to intuitively predict the location of hard and soft material for a spiral and bending actuator.

Future work will incorporate compressibility constraints via the range of r in eq. 3 as a function of the mapping such that each differential volume remains constant under the deformation over the entire space of initial and final shapes. Then we will apply boundary conditions for the pressure through a normal force on the inner cylinder wall and to integrate over the newly-included thickness to achieve the material constants. Additionally, finite element modeling is ongoing in ANSYS to validate the Continuum Mechanics model as well as the dithering operation. While this approach is illustrated for a bending and spiraling actuator, the method can be generalized to other shapes as well given a suitable parameterization of the shapes and their spine.

This early model shows potential to design pre-specified shapes by dithering two distinct materials about the actuator body. In doing so this model holds the possibility of creating patient-specific actuators for use in a catheter robot.

VI. Acknowledgments

We would like to thank the MnDRIVE Robotics, Sensors, and Advanced Manufacturing initiative for financial support.

References

[1] D. Rus and M. T. Tolley, "Design, fabrication and control of soft robots," *Nature*, vol. 521, no. 7553, pp. 467–475, May 2015.

[2] A. Stilli, H. A. Wurdemann, and K. Althoefer, "Shrinkable, stiffness-controllable soft manipulator based on a bio-inspired antagonistic actuation principle," in *Intelligent Robots and Systems (IROS 2014), 2014 IEEE/RSJ International Conference on*. IEEE, 2014, pp. 2476–2481.

[3] J. Bishop-Moser and S. Kota, "Design and modeling of generalized fiber-reinforced pneumatic soft actuators," *IEEE Trans. Robot.*, vol. 31, no. 3, pp. 536–545, June 2015.

[4] P. E. Dupont, J. Lock, B. Itkowitz, and E. Butler, "Design and control of concentric-tube robots," *IEEE Transactions on Robotics*, vol. 26, no. 2, pp. 209–225, 2010.

[5] H. B. Gilbert, D. C. Rucker, and R. J. Webster III, "Concentric tube robots: The state of the art and future directions," in *Robotics Research*. Springer, 2016, pp. 253–269.

[6] M. D. Gilbertson, G. McDonald, G. Korinek, J. D. Van de Ven, and T. M. Kowalewski, "Serially actuated locomotion for soft robots in tube-like environments," *Robotics and Automation Letters, IEEE*, vol. 2, no. 2, pp. 1140–1147, January 2017.

[7] A. Goriely and M. Tabor, "Rotation, inversion and perversion in anisotropic elastic cylindrical tubes and membranes," in *Proc. R. Soc. A*, vol. 469, no. 2153. The Royal Society, 2013, p. 20130011.

[8] F. Connolly, C. J. Walsh, and K. Bertoldi, "Automatic design of fiber-reinforced soft actuators for trajectory matching," *Proceedings of the National Academy of Sciences*, vol. 114, no. 1, pp. 51–56, 2017.

[9] R. Floyd and L. Steinberg, "An adaptive algorithm for spatial grey scale," *Proceedings of the Society of Information Display*, 1976.

[10] P. Polygerinos, Z. Wang, J. T. Overvelde, K. C. Galloway, R. J. Wood, K. Bertoldi, and C. J. Walsh, "Modeling of soft fiber-reinforced bending actuators," 2015.